Electronic Supplementary Material (ESI) for Journal of Materials Chemistry A.

Iron-doped NASICON Type Sodium Ion Battery Cathode for Enhanced Sodium Storage Performance and Its Full Cell Applications

Jae Yeol Park,[a] Yoonsu Shim,[a] Yong-il Kim,[b] Yuseon Choi,[c] Ho Jun Lee,[a] Jungjae Park,[a] Ji Eun Wang,[a] Yonghee Lee,[d] Joon Ha Chang,[a] Kanghoon Yim,[e] Chi Won Ahn,[d] Chan-Woo Lee,[e] Do Kyung Kim,[a] and Jong Min Yuk [a]*

[a] Department of Materials Science & Engineering, Korea Advanced Institute of Science and Technology (KAIST), 291 Daehak-ro, Yuseong-gu, Daejeon, 34141, Republic of Korea.
[b] Korea Research Institute of Standards and Science, 267 Gajeong-ro, Yuseong-gu, Daejeon, Republic of Korea.
[c] Department of Chemical Engineering, Konkuk University, 120 Neungdong-ro, Gwangjin-gu, Seoul, Republic of Korea.
[d] National Nano Fab Center (NNFC), 291 Daehak-ro, Yuseong-gu, Daejeon, 34141, Republic of Korea.
[e] Platform Technology Laboratory, Korea Institute of Energy Research, Daejeon, 152 Gajeong-ro, Yuseong-gu, 34129, Republic of Korea.

Methods

Materials preparation

NVPF/NVP and transition metal substituted NVPF/NVP are synthesized by conventional sol-gel method [1]. For NVPF/NVPs (Fe 0 %, 4.9 %, 8.9 %, 11.5 %, 14.8 %), Ammonium metavanadate (NH_4VO_3, 2.00, 1.80, 1.65, 1.60, and 1.50 mmol), iron nitrate (0, 0.20, 0.35, 0.40, and 0.50 mmol), ammonium phosphate ($NH_4H_2PO_4$, 2.00 mmol), sodium fluoride (NaF, 3.00 mmol), and citric acid ($C_6H_8O_7$, 1.6 mmol) are added in DI water. For NVPF/NVPs (Ti 2.8 %, Cu 3.6 %, Zn 1.9 %, Cr 1.9 %, Mn 2.6%), TiO and metal nitrates (0.15 mol, 0.15 mol, 0.10 mol, 0.10 mol, 0.10 mol, and 0.10 mol, respectively) are used instead of iron nitrate. The real content of the transition metals in NVPF/NVP is confirmed with inductively coupled plasma (ICP). The prepared solution is heated at 80 ^oC until it presents a blue color. The blue solution is dried in 80 ^oC in the vacuum oven until it becomes a gel and completely dried overnight at 120 ^oC. The dried gel is ground, pelletized, and heated at 300 ^oC and 650 ^oC for 4 h and 8 h in Ar atmosphere. For CuS, bulk CuS (100 mesh) is purchased from Sigmaaldrich.

Materials characterization

Transmission electron microscopes (TEM, JEM 3010, ARM 200F, JEOL) and XRD are employed to investigate morphology and crystal structure. X-ray photoelectron spectroscopy (XPS, K-Alpha+, ThermoFisher scientific) is used to analyse the valence state of O, F, Fe, V. XPS analysis is conducted after shifting the spectra so that peaks corresponding C-C bonds are located at 284.8 eV. The XRD patterns are obtained with RIGAKU smartlab, and the patterns are refined with the space group of $P4_2/mmm$, $R\bar{3}c$, and $P2_1/c$ for $Na_3V_{2-x}Fe_x(PO_4)_2F_3$, $Na_3V_{2-x}Fe_x(PO_4)_3$, and $Na_5V_{1-x}Fe_x(PO_4)_2F_2$ phases using Total Pattern Analysis Solution (TOPAS, Bruker AXS) software. For the refinement, uniform V/Fe ratio for the three phases is assumed. In-situ small angle x-ray scattering (D/MAX-2500 with R-AXIS IV++ diffractometer, Rigaku) is employed to investigate the crystal structural evolutions of NVPF/NVPs (Fe 0 %, Fe 8.9 %). Electron-beam is irradiated on a rotating anode type Cu plate at 50kV and 100mA to generate the X-ray beam (Cu k alpha). The X-ray beam is filtered through a slit of a diameter of 0.15 mm and collimated into a hole-punched coin-cell. The hole is well sealed with polymer membrane. The data is acquired at hourly intervals. The obtained 2D intensity maps are converted into 1D spectra by summing the intensity and normalized for radial directions. RigakuDisplay software is employed for the data processing.

Electrochemical characterization

To fabricate the working electrode, slurry containing active materials, carbon black (acetylene black, Alfa Aesar), and polyvinylidene fluoride (PVDF, Sigma Aldrich) is prepared with 1-methyl-2-pyrrolidone. The ratios among active materials, carbon black and PVDF are 8:1:1 and 7:2:1 for anode and cathode, respectively. The slurry is coated on a Cu foil and Al foil in anode and cathode cases, respectively. The coated anode and cathode electrodes are dried at 80 ^oC and 120 ^oC, respectively, in a vacuum oven. For electrolyte, 1M $NaPF_6$ in diglyme is used [2-4]. For half cell test, a pure Na foil (Sigma Aldrich) and glass fiber (GF/F, Whatman) are employed for a counter electrode and separator, respectively. For full cell test, anode and cathode are combined with mass ratio of ~ 3.43:1. The bulk CuS is pre-cycled before full cell configuration. 2032 type coin cell and swagelok cell (ECC-STD, EL-CELL) are employed for cycling test and cyclic voltammetry, respectively. Galvanostatic cell test is performed using a battery cycling system (WBCS 3000L, Wonatech). Cyclic voltammetry is conducted with a potentiostat (PARSTAT MC 1000, Princeton Applied Research). All the electrochemical tests are performed at room temperature.

Computational analysis

The band structures of NVPF and Fe-doped NVPF are calculated with density functional theory (DFT) method employing the Vienna *Ab initio* Simulation Package (VASP) [5] within the projector-augmented wave (PAW) scheme as formulated by Perdew-Burke-Ernzerhof (PBE) [6] with spin-polarization. A cutoff energy of 500 eV is adopted for the plane-wave expansion of wave functions, and the Brillouin zone integrations are carried out with *k*-point mesh of 4 × 4 × 3 with the Gamma-centered method. A Hubbard *U* terms of 3.1 eV and 4.0 eV are chosen for V and Fe based on previous studies [7-10]. The energies in the calculation are converged within 1.0×10^{-6} eV. The atomic structure is based on the Materials Project [11], which is fully relaxed using above-mentioned parameters and well matches with previous DFT studies (Table S1). The atomic modes are drawn with VESTA software [12].

Supplementary Figures

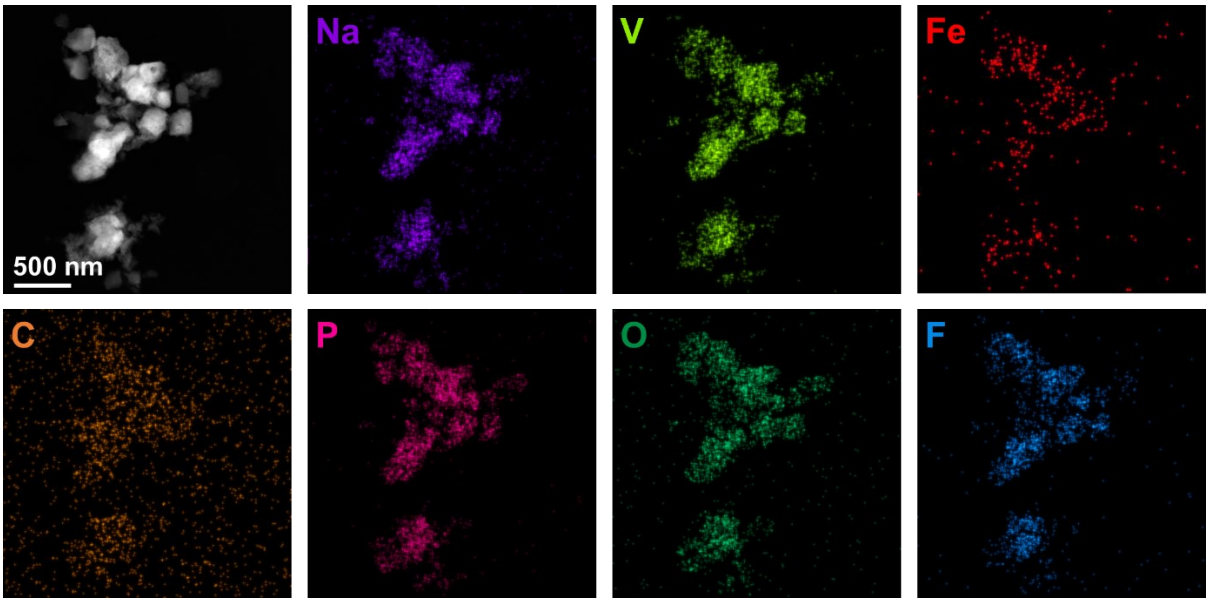

Figure S1. Energy dispersive spectroscopy (EDS) map of NVPF/NVP (Fe 8.9 %).

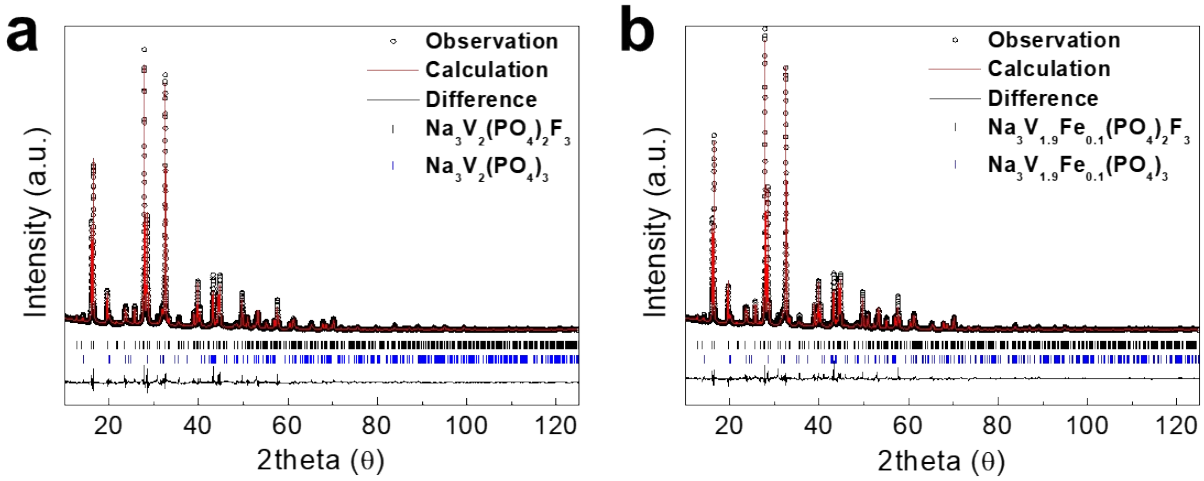

Figure S2. Rietveld refinement of NVPF/NVPs (Fe **(a)** 0, **(b)** 4.9%)

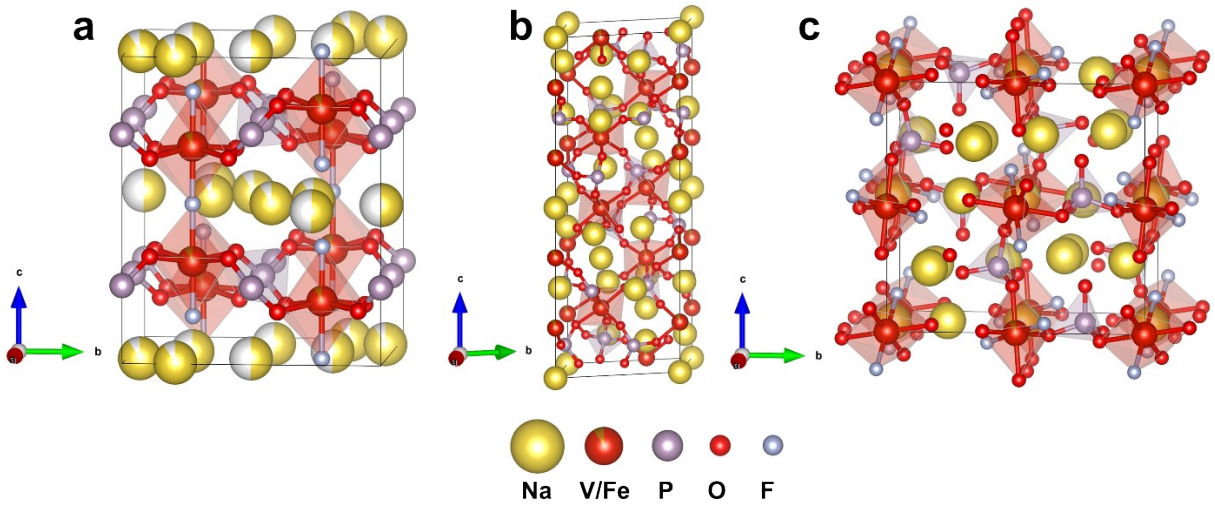

Figure S3. Crystal structures of (a) $Na_3V_{1.82}Fe_{0.18}(PO_4)_2F_3$, **(b)** $Na_3V_{1.82}Fe_{0.18}(PO_4)_3$, and **(c)** $Na_5V_{0.91}Fe_{0.09}(PO_4)_2F_2$. The crystal structures of the two major phases in NVPF (Fe 0, 4.9%) are similar to crystal structures in (a) and (b).

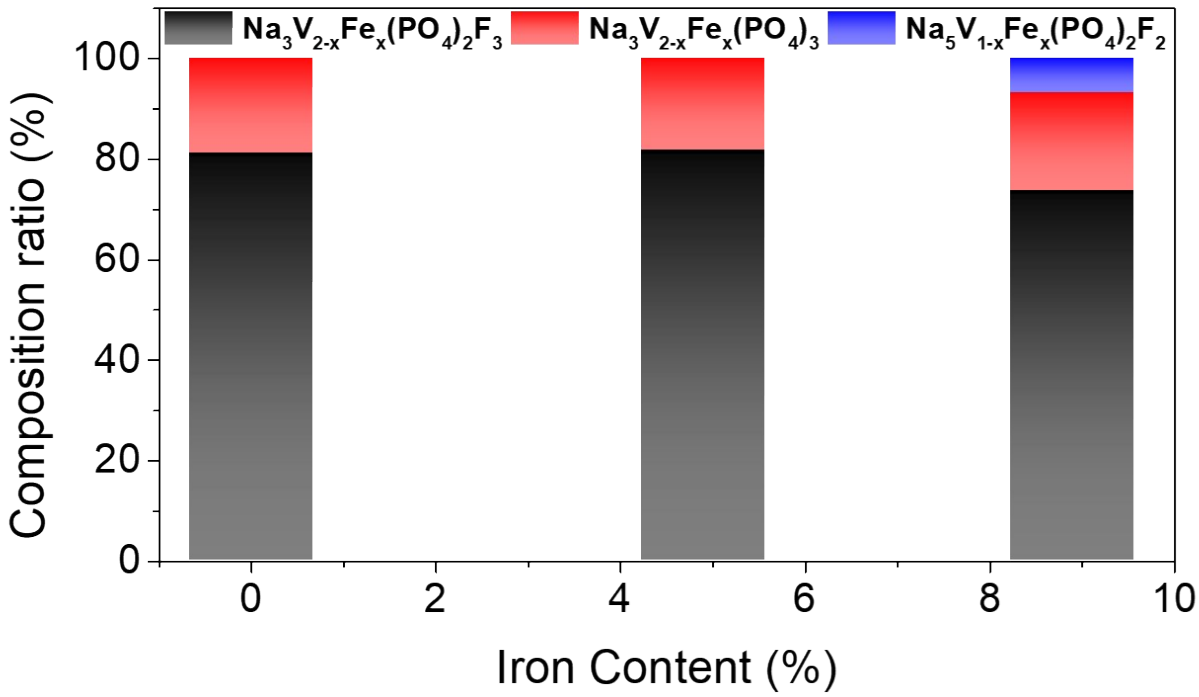

Figure S4. Phase ratios in a function of Fe content obtained by Rietveld refinement.

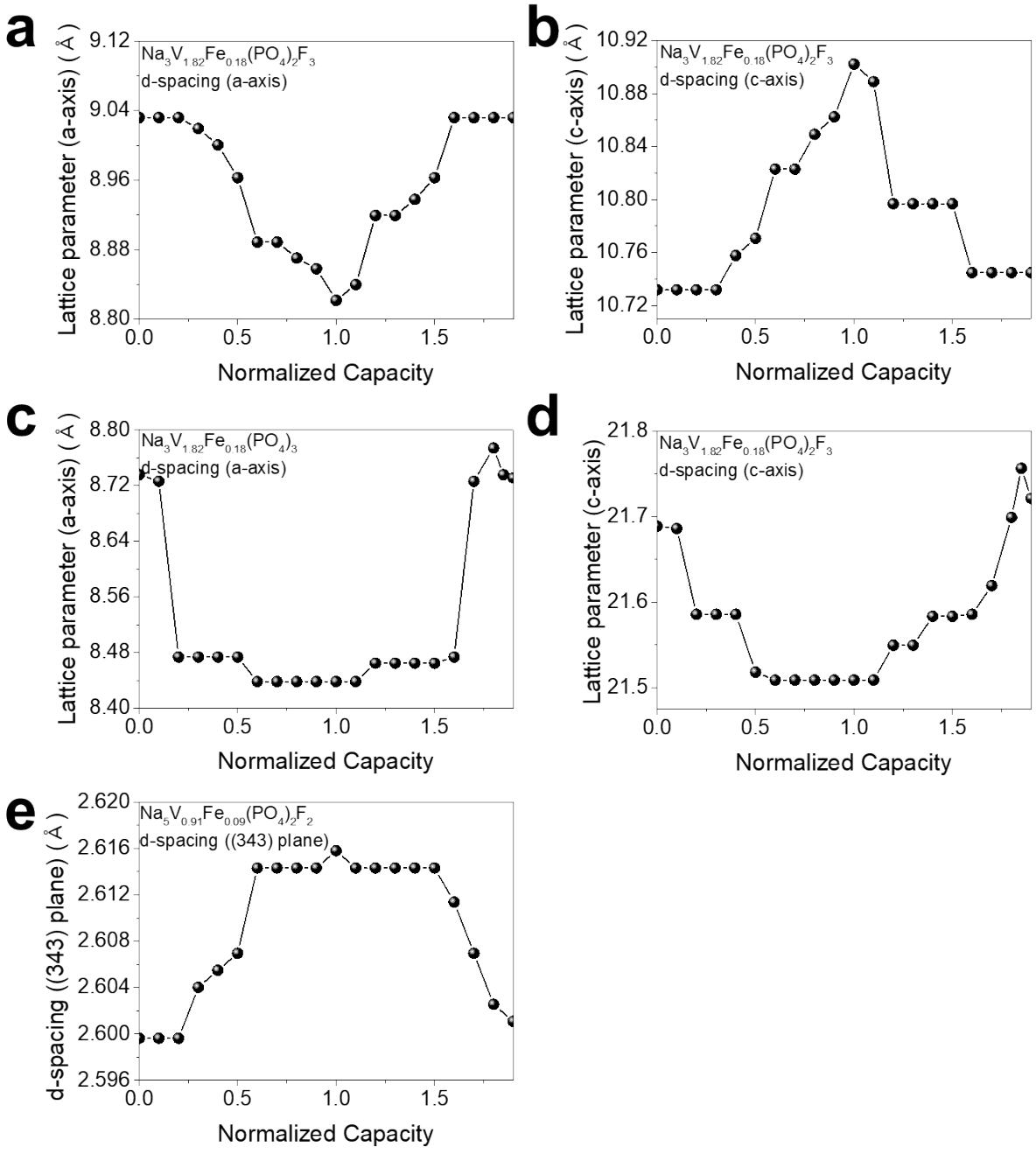

Figure S5. Lattice parameter and d-spacing changes of (a)(b) $Na_3V_{1.82}Fe_{0.18}(PO_4)_2F_3$ and **(c)(d)** $Na_3V_{1.82}Fe_{0.18}(PO_4)_3$, and **(e)** d-spacing ((004) plane) change of $Na_5V_{0.91}Fe_{0.09}(PO_4)_2F_2$.

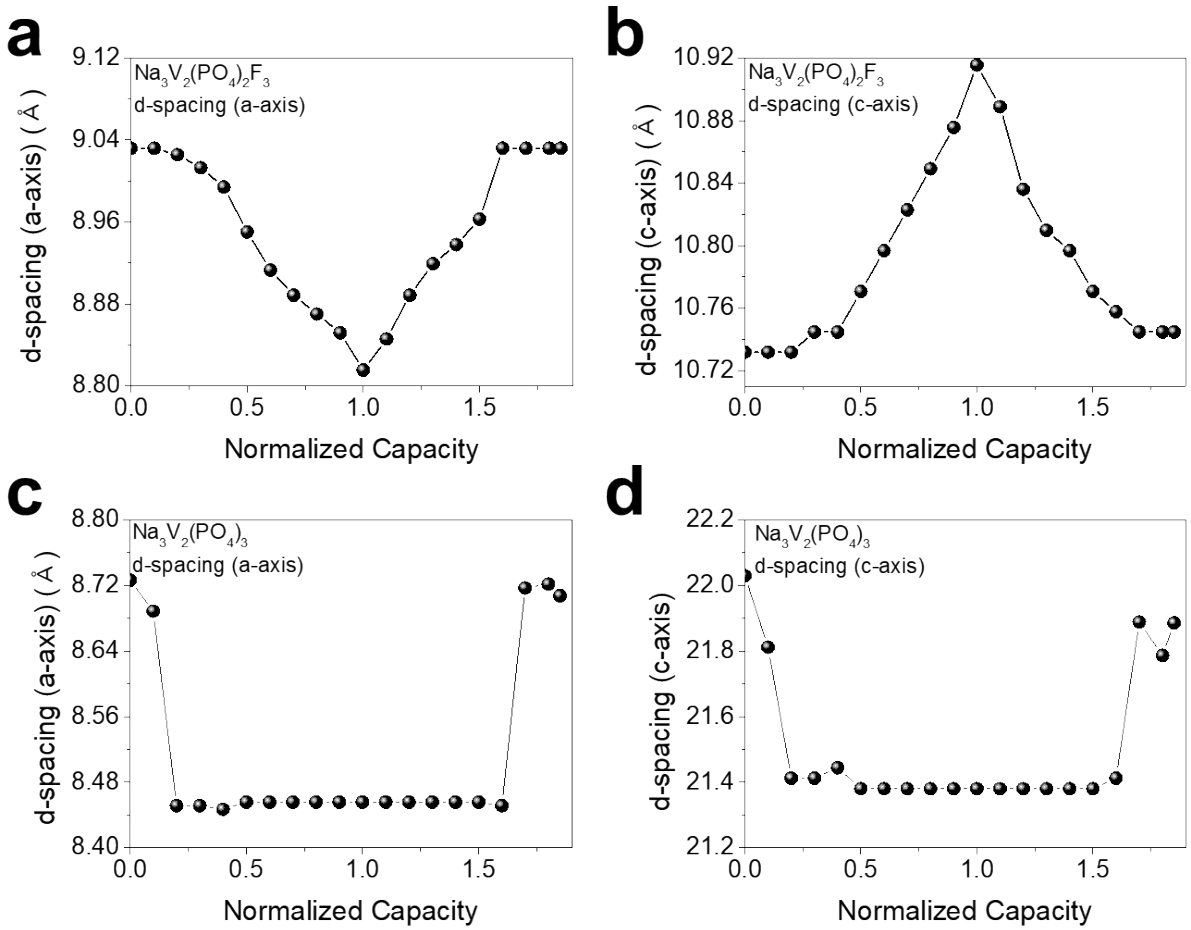

Figure S6. Lattice parameter changes of (a)(b) $Na_3V_2(PO_4)_2F_3$ and **(c)(d)** $Na_3V_2(PO_4)_3$.

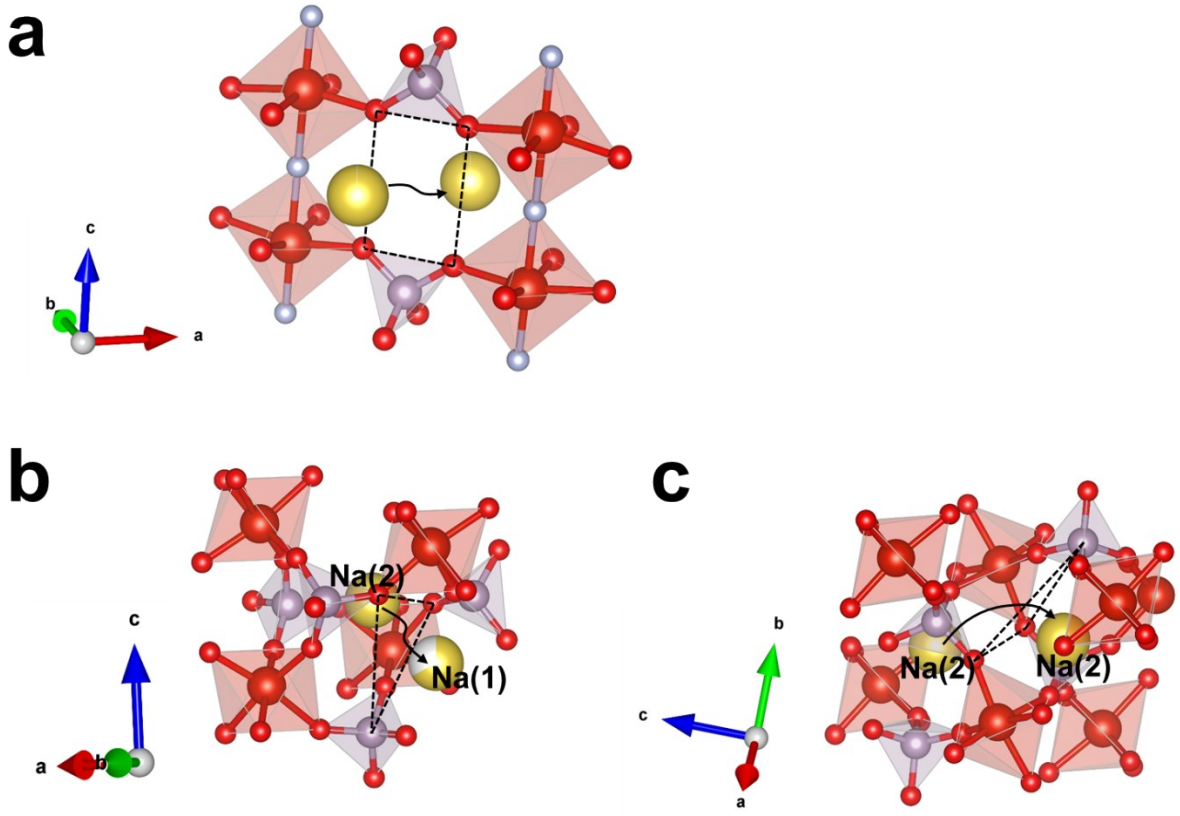

Figure S7. Sodium migration paths in (a) $Na_3V_2(PO_4)_2F_3$, (b)(c) $Na_3V_2(PO_4)_3$.

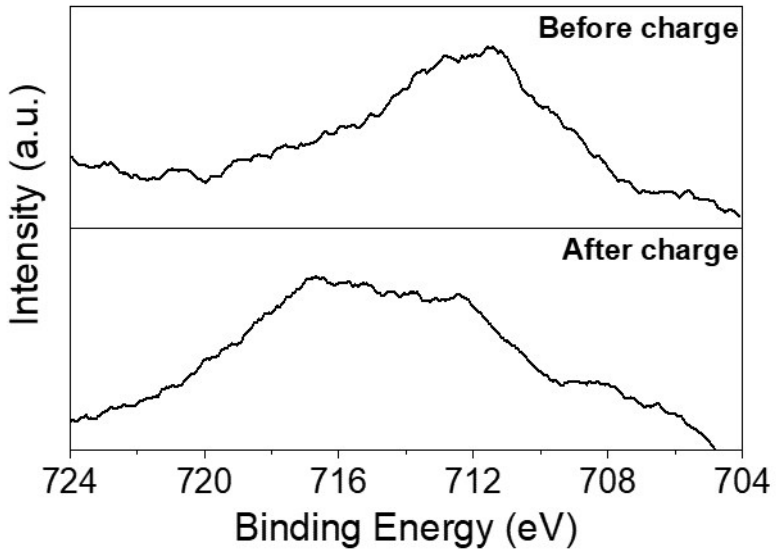

Figure S8. Valence changes of Fe in NVPF/NVP (8.9 %). Peak shift of Fe2p spectrum to over ~ 716 eV in NVPF/NVP (Fe 8.9 %) implies that Fe^{3+} is oxidized to Fe^{4+}.

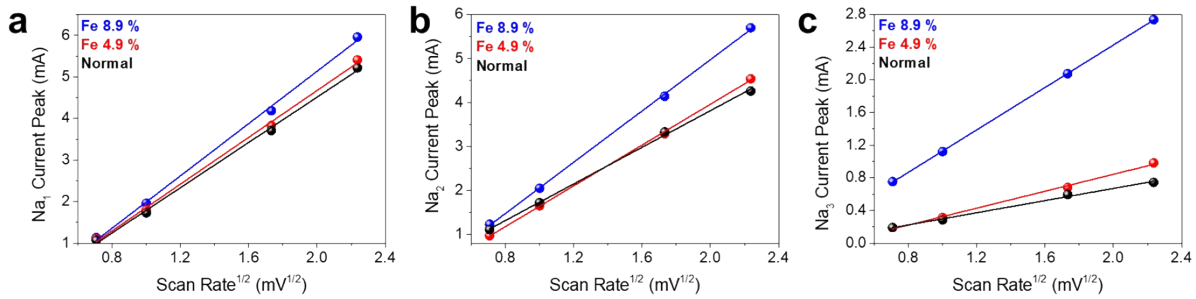

Figure S9. Linear plot of current peaks of NVPF/NVPs (Fe 0, 4.9 %, 8.9 %) as a fuction of voltage scan rate$^{1/2}$ at (a) the first plateau (~ 4.15 V), **(b)** second plateaus (~ 3.65 V), and **(c)** third plateau (~ 3.36 V).

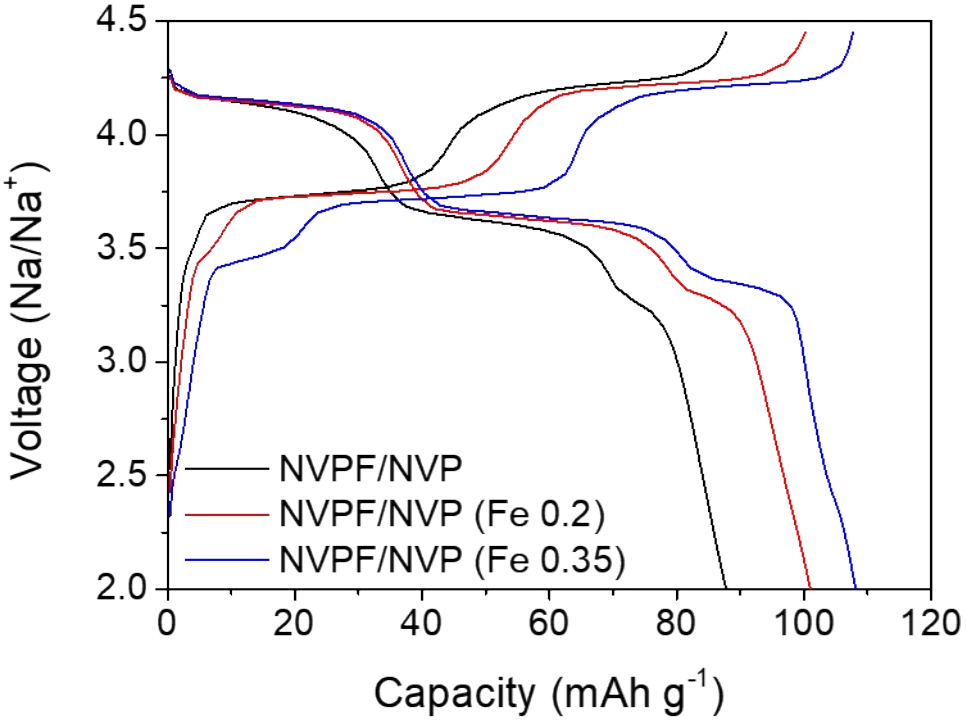

Figure S10. Charge and discharge profiles of NVPF/NVPs (Fe 0 %, 4.9 %, 8.9 %) at 10 C.

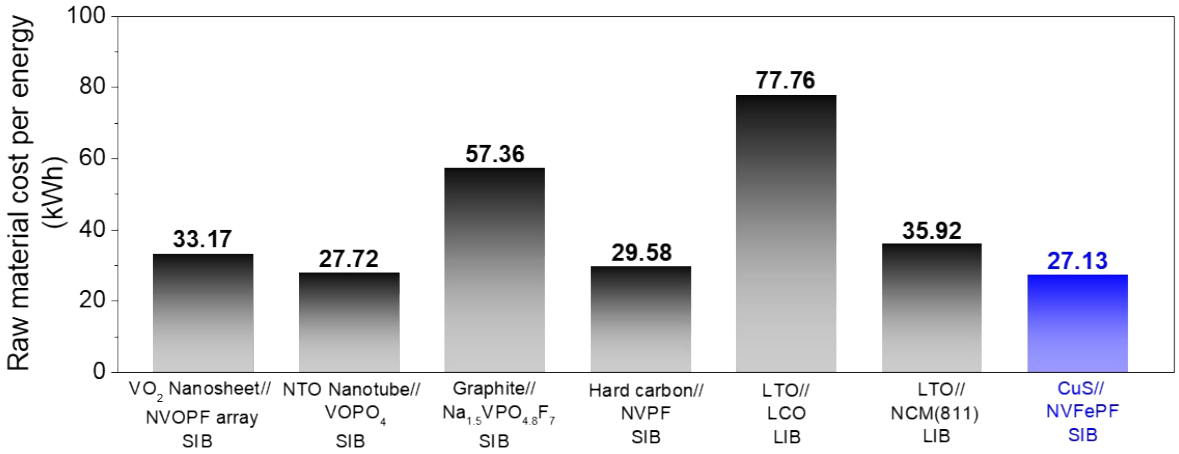

Figure S11. Comparison of the cost per theoretical energy in NVPF/NVP (Fe 8.9 %) - CuS full cell with previously reported SIBs and commercialized LIBs. NTO, $Na_{1.5}VPO_{4.8}F_{0.7}$, LCO, and NCM (811) indicate $Na_2Ti_3O_7$, $Na_3V_2(PO_4)_2O_{1.4}F_{1.6}$, $LiCoO_2$, $Li(Ni_{0.8}Co_{0.1}Mn_{0.1})O_2$, respectively. The detailed information to get the values are presented in Table S3.

Table S1. Prices for the raw materials obtained from [a] Korea mineral resources information service, [b] United state geological survey, [c] Shanghai metal market, and [d] Alibaba. The prices are based on Aug. 2020.

Materials	Price (usd/ton)
V_2O_5	13,500[a]
$CoSO_4\ 7H_2O$	6,545[c]
$NiSO_4\ 6H_2O$	3,640[c]
TiO_2	990[b]
$MnSO_4$	784[c]
Ferrochrome (low carbon)	3,800[a]
$CuSO_4$	1,943[c]
Zn	2,466.5[a]
Fe(NO3)3 9H2O	750[a]
Li_2CO_3	5,775[a]

Table S2. Lattice parameters of $Na_3V_2(PO_4)_2F_3$ calculated from DFT (GGA+U) in comparison with the previous work [7].

Sample	Method	*a* (Å)	*b* (Å)	*c* (Å)	vol. (Å^3)
$Na_3V_2(PO_4)_2F_3$	DFT (This work)	9.132	9.199	10.895	915.21
	DFT [7]	9.15	9.19	10.90	916.56

Table S3. Prices for the raw materials needed for anode and cathode materials obtained from [a] Korea mineral resources information service, [b] United state geological survey, and [c] Shanghai metal market, [d] Vanadium Price.com, and [e] Alibaba based on Aug. 2020. For the vanadium source in cathode, V_2O_5 is considered instead of NH_4VO_3, which is source for producing V_2O_5, due to difficulty of finding price information. Normal Ti metal powder is considered instead of Ti nano powder.

Anode/element	Theoretical/practical capacity (mAh g^{-1})	Average charge/discharge voltage (V)	Raw material	Raw material price	Price (usd/ton)
$Li_4Ti_5O_{12}$	175	1.6			2294.1
Li			Li_2CO_3	4830[a]	
Ti			TiO_2	850[b]	
CuS	560	1.55			3262.8
Cu			$CuSO_4$ $5H_2O$	2082[c]	
S			S	60[b]	
VO_2 nanosheet	431 (Na storage)	0.831			37,853
			VOC_2O_4	20,000[e]	
$Na_2Ti_3O_7$ nanotube	234 (Na stoage)	0.766			4,865
Ti			Ti powder	10000[e]	
Na			NaOH	360[e]	
Graphite	372 (Li storage) 130 (Na storage)	0.1 1.025			10000[13]
Standard hard carbon	300 (Na storage)	0.215			15000[13]

Cathode/element	Theoretical/practical capacity		Raw material	Raw material price	Price (usd/ton)
NVOPF array	130	3.6			6558
Na, F			NaF	800[e]	
V			V_2O_5	13,666[d]	
PO4			$NH_4H_2PO_4$	650[e]	
Na, O			Na_2CO_3	300[e]	
$Na_3V_2(PO_4)_2O_{1.6}F_{1.4}$	120	3.67			6608
Na, F			NaF	800[e]	
V			V_2O_5	13666[d]	
PO4			$NH_4H_2PO_4$	650[e]	
Na, O			Na_2CO_3	300[e]	
NVPF/NVP (Fe 8.9 %)	120	3.64			6079
Na, F			NaF	800[e]	
V			V_2O_5	13,666[d]	
PO_4			$NH_4H_2PO_4$	650[e]	
Fe			$FeSO_4$ $7H_2O$	750[e]	
LCO ($LiCoO_2$)	150	~ 3.7			22330
Li			Li_2CO_3	4830[a]	
Co			$CoSO_4$ $7H_2O$	7140[c]	
NCM(811) ($Li(Ni_{0.8}Co_{0.1}Mn_{0.1})O_2$)	205	~ 3.7			12508
Li			Li_2CO_3	4830[a]	
Ni			$NiSO_4$ $6H_2O$	3850[c]	
Co			$CoSO_4$ $7H_2O$	7140[c]	
Mn			$MnSO_4$	805[c]	

Table S4. Theoretical comparison among CuS-NVPF/NVP (Fe 8.9 %), conventional LTO-LCO and LTO-NCM (811) full cell in cost and performance aspects.

Assumption

1) Full cell capacity = 3000 mAh
2) Anode and cathode capacity ratio = 1.1
3) Gravimetric capacity is based on total electrodes mass.
4) Capacity of NVPF/NVP (Fe 8.9 %), LCO, and NCM (811) = 120 mAh g^{-1}, 150 mAh g^{-1}, and 205 mAh g^{-1}.
5) Capacity of CuS and LTO = 560 mAh g^{-1} and 175 mAh g^{-1}
6) Average discharge voltage of the cathodes = 3.7 V for LCO and NCM, and 3.67 V for NVPF/NVP (Fe 8.9 %)
7) Average charge voltage of CuS and LTO = 1.55 V and 1.6 V

Anode/cathode combination	Required cathode mass (g)	Required anode mass (g)	Energy density (Wh kg^{-1})	Required raw materials cost (usd)
LTO-LCO	20	18.9	162.13	0.490
LTO-NCM (811)	14.6	18.9	188.11	0.226
CuS-NVPF/NVP (Fe 8.9%)	25	5.9	205.87	0.173

Reference

1 Liu, Q. *et al.* Carbon-coated $Na_3V_2(PO_4)_2F_3$ nanoparticles embedded in a mesoporous carbon matrix as a potential cathode material for sodium-ion batteries with superior rate capability and long-term cycle life. *Journal of Materials Chemistry A* **3**, 2015, 21478-21485.

2 Kim, H. *et al.* Sodium Storage Behavior in Natural Graphite using Ether-based Electrolyte Systems. *Advanced Functional Materials* **25**, 2015, 534-541.

3 Park, J. Y. *et al.* Atomic visualization of a non-equilibrium sodiation pathway in copper sulfide. *Nature Communications* **9**, 2018, 922.

4 Park, J. Y. *et al.* Pulverization-Tolerance and Capacity Recovery of Copper Sulfide for High-Performance Sodium Storage. *Advanced Science* **6**, 2019, 1900264.

5 Kresse, G. & Furthmüller, J. Efficient iterative schemes for ab initio total-energy calculations using a plane-wave basis set. *Physical Review B* **54**, 1996, 11169-11186.

6 Perdew, J. P., Burke, K. & Ernzerhof, M. Generalized Gradient Approximation Made Simple. *Physical Review Letters* **77**, 1996, 3865-3868.

7 Dacek, S. T., Richards, W. D., Kitchaev, D. A. & Ceder, G. Structure and Dynamics of Fluorophosphate Na-Ion Battery Cathodes. *Chemistry of Materials* **28**, 2016, 5450-5460.

8 Liu, Z. *et al.* Local Structure and Dynamics in the Na Ion Battery Positive Electrode Material $Na_3V_2(PO_4)_2F_3$. *Chemistry of Materials* **26**, 2014, 2513-2521.

9 Wang, L., Maxisch, T. & Ceder, G. Oxidation energies of transition metal oxides within the $\mathrm{GGA}+\mathrm{U}$ framework. *Physical Review B* **73**, 2006, 195107.

10 Park, Y.-U. *et al.* A Family of High-Performance Cathode Materials for Na-ion Batteries, $Na_3(VO_{1-x}PO_4)_2\ F_{1+2x}$ $(0 \le x \le 1)$: Combined First-Principles and Experimental Study. *Advanced Functional Materials* **24**, 2014, 4603-4614.

11 Jain, A. *et al.* Commentary: The Materials Project: A materials genome approach to accelerating materials innovation. *APL Materials* **1**, 2013, 011002.

12 Momma, K. & Izumi, F. VESTA 3 for three-dimensional visualization of crystal,

volumetric and morphology data. *Journal of Applied Crystallography* **44**, 2011, 1272-1276.

13 Vaalma, C., Buchholz, D., Weil, M. & Passerini, S. A cost and resource analysis of sodium-ion batteries. *Nature Reviews Materials* **3**, 2018, 18013.